



Novel Pyrrolidine Diketopiperazines Selectively Inhibit Melanoma Cells via Induction of Late-Onset Apoptosis

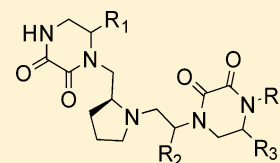
Lillian Onwuha-Ekpete,[†] Lisa Tack,[†] Anna Knapinska,[†] Lyndsay Smith,[†] Gaurav Kaushik,[‡] Travis LaVoi,[†] Marc Giulianotti,[†] Richard A. Houghten,[†] Gregg B. Fields,[†] and Dmitriy Minond^{*,†}

[†]Torrey Pines Institute for Molecular Studies, 11350 South West Village Parkway, Port St. Lucie, Florida 34987, United States

[‡]University of Kansas Medical Center, 3901 Rainbow Boulevard, Kansas City, Kansas 66160, United States

S Supporting Information

ABSTRACT: A common liability of cancer drugs is toxicity to noncancerous cells. Thus, molecules are needed that are potent toward cancer cells while sparing healthy cells. The cost of traditional cell-based HTS is dictated by the library size, which is typically in the hundreds of thousands of individual compounds. Mixture-based combinatorial libraries offer a cost-effective alternative to single-compound libraries while eliminating the need for molecular target validation. Presently, lung cancer and melanoma cells were screened in parallel with healthy cells using a mixture-based library. A novel class of compounds was discovered that selectively inhibited melanoma cell growth via apoptosis with submicromolar potency while sparing healthy cells. Additionally, the cost of screening and biological follow-up experiments was significantly lower than in typical HTS. Our findings suggest that mixture-based phenotypic HTS can significantly reduce cost and hit-to-lead time while yielding novel compounds with promising pharmacology.



One of the most common liabilities of cancer drugs/drug candidates is toxicity to noncancerous cells. Thus, molecules are needed that are potent toward cancer cells and spare healthy cells. Cell-based high-throughput screening (HTS) approaches can be used to discover such molecules. Unfortunately, the cost of HTS limits the amount and number of cell lines that can be screened in parallel in order to discover molecules with desired activity/toxicity profiles. The cost of traditional cell-based HTS is dictated by the HTS library size, which is typically in the hundreds of thousands or millions of individual compounds. This means that hundreds of thousands of wells need to be screened against at least two different cell lines (one cancerous and one healthy) to assess diverse chemical space in order to find potential leads.

Mixture-based combinatorial libraries offer a cost-effective alternative to single-compound libraries,¹ especially when it comes to parallel screening of multiple targets/cell lines. The significantly reduced sample numbers utilized with a mixture-based combinatorial library screening approach eliminates the need for the molecular target validation typically needed prior to large-scale HTS campaigns and allows one to probe cancer cells directly in an agnostic, target-unbiased fashion.² A recent review by Swinney and Anthony³ showed that more first-in-class drugs came from phenotypic screening (i.e., cell- or organism-based) than from target-based screening.

Drug resistance is a major challenge of cancer drug discovery. Cancer can be de novo resistant to a particular drug or acquire resistance to it after a prolonged therapy. Monotherapy using drugs derived from target-based drug discovery has been shown to result in acquired resistance by cancer cells. For example, the recently approved inhibitor of V600E BRAF, vemurafenib, demonstrated increased survival of patients with metastatic melanoma, but after 6–8 months of therapy, resistance

occurred.⁴ Given the propensity of single-target-based compounds to cause resistance, a potential of phenotypic screening to discover compounds that favorably interact with multiple targets (i.e., polypharmacology),^{5,6} thus avoiding or diminishing the chances for resistance, represents an additional benefit as compared to the target-based screening.

The above considerations prompted us to screen our in-house mixture-based druglike library¹ to discover potentially first-in-class selective inhibitors of various cancers to demonstrate the utility of mixture-based libraries. To assess our library for inhibition of growth of drug-resistant cancer cells, we chose two of the most lethal cancer types: lung cancer and melanoma. NRAS mutation is one of the most common mutations exhibited in melanoma and is present in 95% of patients of familial melanoma. Therefore, we chose the M14 melanoma cell line as a representative of cutaneous malignant melanoma carrying NRAS but not BRAF mutation.⁷ Additionally, we screened our library against an A549 nonsmall cell lung cancer cell line harboring KRAS mutation⁸ and a healthy control CHO-K1 cell line.

RESULTS AND DISCUSSION

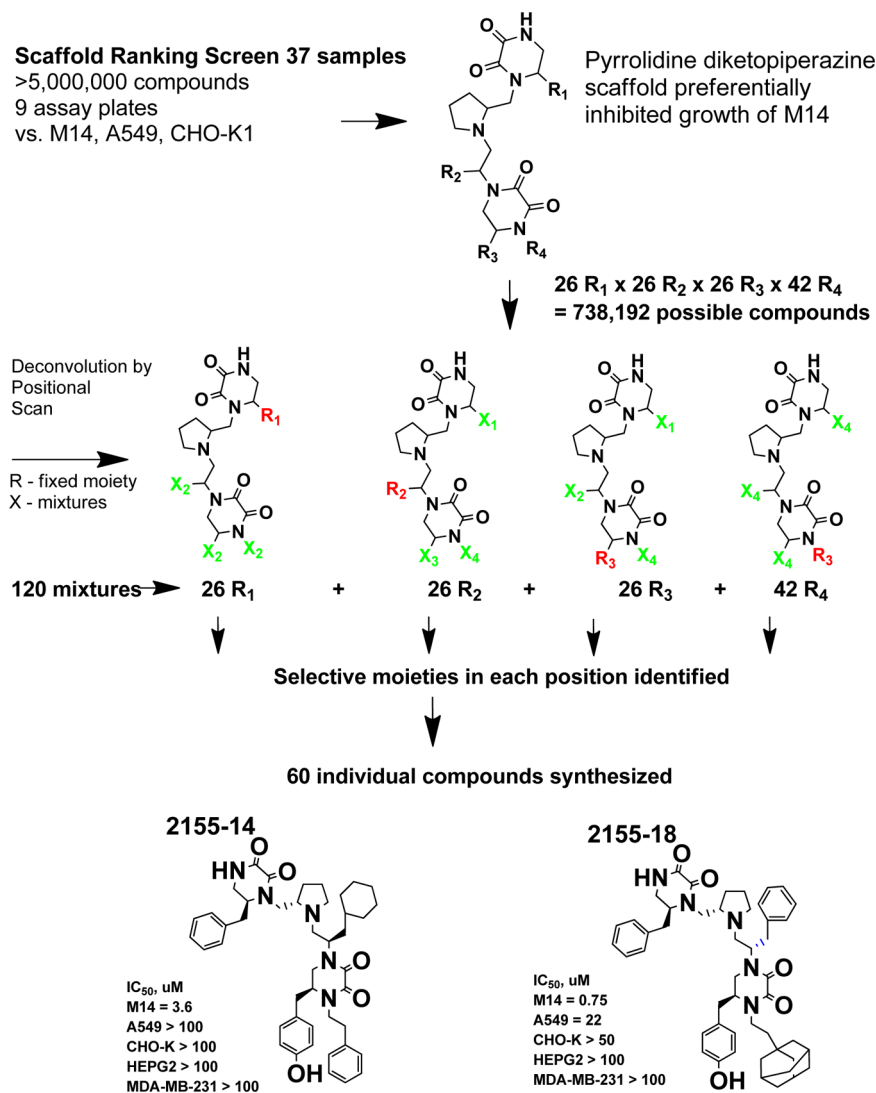
TPIMS Mixture Library Screen. Our group has previously described the mixture-based library screening work flow employed in this work for the identification of novel ligands of various targets,^{9–13} which we have summarized in Scheme 1. The approach allows us to systematically assess >5 000 000 compounds through the use of approximately 200 samples to identify lead individual compounds while accumulating valuable SAR data at each step. The first step in the process involves the

Received: December 19, 2013

Published: January 28, 2014



Scheme 1. Deconvolution of Pyrrolidine Diketopiperazine Library



screening of the 37 mixture samples contained in the scaffold-ranking library.^{1,11–13} As a result of this screen, one mixture library (TPI1344) exhibited selective inhibition of M14 cell line viability (Figure 1A), whereas no effect was seen on viability of A549 and CHO-K1 cells. The basic scaffold of mixture library 1344 consists of two diketopiperazine moieties connected via central pyrrolidine (Figure 1B). To identify individual selective inhibitors from mixture library 1344, a structure–activity relationship study was conducted using a positional scan approach. A positional scan is a screen of a systematically formatted collection of compounds that allows for the rapid identification of the active functionalities around a core scaffold.^{1,14,15} The basic scaffold of library 1344 (Figure 1B), composed of 738 192 ($26 \times 26 \times 26 \times 42$) members, has four sites of diversity (R_1 , R_2 , R_3 , and R_4) and therefore is made up of four separate sublibraries, each having a single defined position (R) and three mixture positions (X). Screening the four sets of mixtures, totaling 120 mixtures ($26 + 26 + 26 + 42$), against chosen cell lines provides information leading to the identification of individual compounds in library 1344 that are active and selective.¹ Each mixture was screened at a final assay concentration of 0.1 mg/mL (13.3 μ M) in triplicate.

Eighteen moieties were identified (Figure 2 and Supporting Information Table 1) that did not significantly inhibit growth of the healthy cell line (CHO-K1). In position R_1 , mixture samples 2 (*S*-benzyl), 9 (*R*-2-naphthylmethyl), and 17 (*R*-methyl) inhibited growth of M14 and A549 cells in the range of 80–98% (Figure 2A). Their stereoisomers (19, 10, and 7, *R*-benzyl, *S*-2-naphthylmethyl, and *S*-methyl, respectively) inhibited all three cell lines equipotently.

In position R_2 , 28 (*S*-benzyl), 33 (*(R,R)*-1-hydroxyethyl), 35 (*S*-4-hydroxybenzyl), 40 (*S*-hydroxymethyl), 41 (*(S,S)*-1-hydroxyethyl), 43 (*R*-4-hydroxybenzyl), and 51 (*R*-cyclohexyl) did not inhibit CHO-K1 cells but were active against both A549 and M14 cell lines. Sample 43 inhibited only M14 cells. Interestingly, samples 33 and 41 (*(R,R)*- and *(S,S)*-1-hydroxyethyl, respectively) and 35 and 43 (*S*-4- and *R*-4-hydroxybenzylethyl, respectively) were stereoisomers. Stereochemistry did not appear to affect CHO-K1 viability. However, in the case of a hydroxybenzyl moiety in the R_2 position (35 and 43), the *R* isomer was much more potent against M14 cells and also was the most selective for M14 cells. Interestingly, *S*-hydroxymethyl (40) was much more selective for CHO-K1 than *R*-hydroxymethyl (32) (Figure 2B).

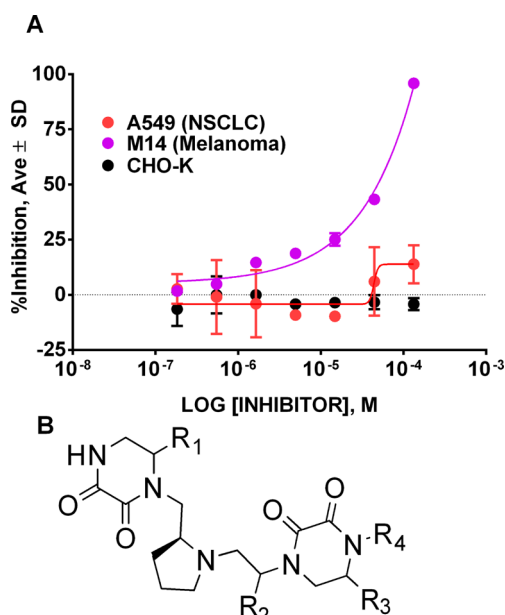


Figure 1. Results of primary screen (scaffold ranking) of TPIMS mixture libraries. (A) Dose response of TP11344 versus A549, M14, and CHO-K cell lines. (B) Core scaffold of TPI1344 mixture library.

In position R₃, seven residues were selective for CHO-K1 cells (Figure 2C). Similarly to R₂, they were mostly

stereoisomers with the exception of 55 (R₃ = hydrogen), 58 and 66 (*R*- and *S*-hydroxymethyl, respectively), 59 and 67 ((*R,R*)- and (*S,S*)-1-hydroxyethyl, respectively), and 61 and 69 (*S*-4- and *R*-4-hydroxybenzyl, respectively). This suggested that position R₃ is the least sensitive to substitutions as far as retaining selectivity for CHO-K1 cells. Only one mixture sample exhibited selectivity toward CHO-K1 cells in position R₄, sample 111 (2-methyl-cyclopropyl)-methyl).

To confirm the selective nature of these 18 mixture samples and to estimate the potency, dose–response experiments were performed using 10-point 3-fold serial dilutions. Mixtures with hydroxybenzyl in positions R₂ (35 and 43) and R₃ (61 and 69) exhibited the most selectivity against CHO-K1 cells (Table 1). Interestingly, 35 (*S*-4-hydroxybenzyl) was not selective against A549 cells, whereas its isomer (43, *R*-4-hydroxybenzyl) was significantly less potent against A549 than M14 cells. Sample 111 ((2-methyl-cyclopropyl)-methyl in the R₄ position) did not confirm selectivity in the dose–response assay.

Synthesis and Evaluation of Individual Compounds.

On the basis of the dose–response experiments with the mixture samples, we synthesized individual compounds containing residues that exhibited selectivity against CHO-K1 cells. Individual compounds with *R*-2-naphthylmethyl (9) and *R*-methyl (17) that were selective as mixtures in the positional scan (Figure 2A) were not selective when present in combination with *S*-4- and *R*-4-hydroxybenzyl in the R₂ and R₃ positions (data not shown). Therefore, several different

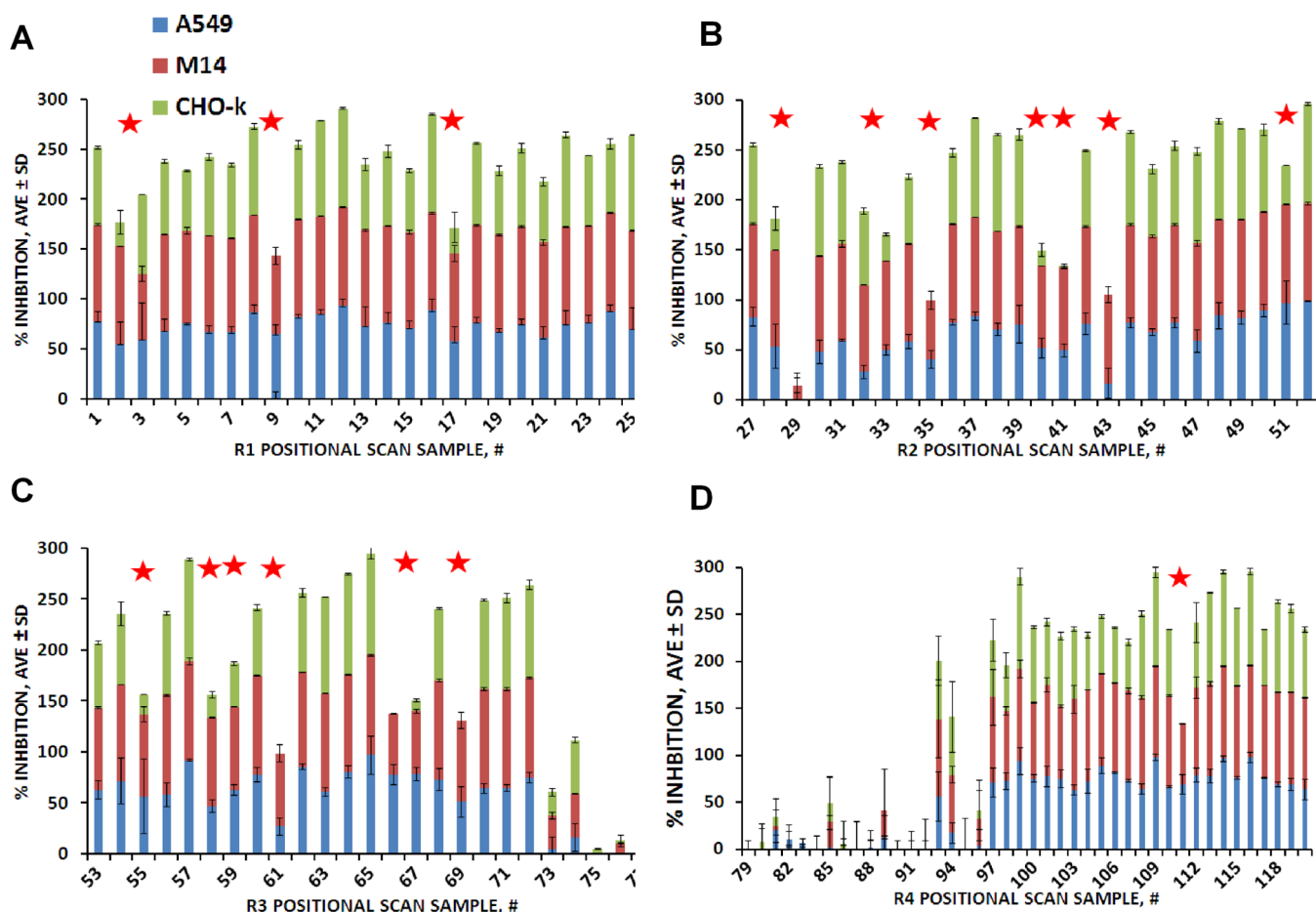
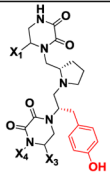
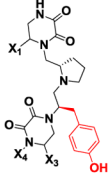
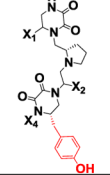
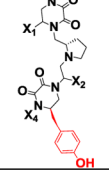
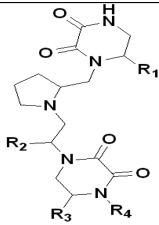


Figure 2. Positional scan of mixture samples to deconvolute scaffold 1344. (A) R₁ scan, (B) R₂ scan, (C) R₃ scan, and (D) R₄ scan. Red stars indicate mixtures that are selective for CHO-K cells.

Table 1. Results of Dose–Response Study of Mixture Samples That Exhibited the Most Selectivity in a Positional Scanning Study of Library 1344^a

Mixture Sample #	Structure	M14	CHO-K1	A549
35		41 ± 5.3	>100	6.0 ± 0.5
43		10 ± 1.3	>100	>100
61		8.0 ± 0.9	>100	>50
69		12 ± 1.5	>100	>50

^aData are reported as the mean of three experiments ± standard deviation. Units are IC₅₀ in micromolar.Table 2. SAR Study Results of Individual Compounds Synthesized on the Basis of a Positional Scan of Library 1344^a

Compound #					Inhibition % @ 100 μM		
	R ₁	R ₂	R ₃	R ₄	A549	M14	CHO-K1
1	R-propyl	S-4-hydroxybenzyl	S-4-hydroxybenzyl	2-phenylbutyl	0	10±1	27±19
2			R-4-hydroxybenzyl	2-phenylbutyl	0	14±3	0
3			S-4-hydroxybenzyl	2-adamantan-1-yl-	19±4	7±1	3±97
4			R-4-hydroxybenzyl	2-adamantan-1-yl-	0	11±3	23±55
5			S-4-hydroxybenzyl	cyclopentyl-methyl	0	15±6	7±5
6			R-4-hydroxybenzyl	cyclopentyl-methyl	5±7	3±21	7±12
7		R-4-hydroxybenzyl	S-4-hydroxybenzyl	2-phenylbutyl	4±1	7±5	48±2
8			R-4-hydroxybenzyl	2-phenylbutyl	8±4	14±21	59±1
9			S-4-hydroxybenzyl	2-adamantan-1-yl-	2±4	12±3	8±9
10			R-4-hydroxybenzyl	2-adamantan-1-yl-	38±5	35±1	77±6
11			S-4-hydroxybenzyl	cyclopentyl-methyl	16±16	23±14	19±1
12			R-4-hydroxybenzyl	cyclopentyl-methyl	14±2	25±16	11±9

^aPercent inhibition data are reported as the mean of three experiments ± standard deviation.

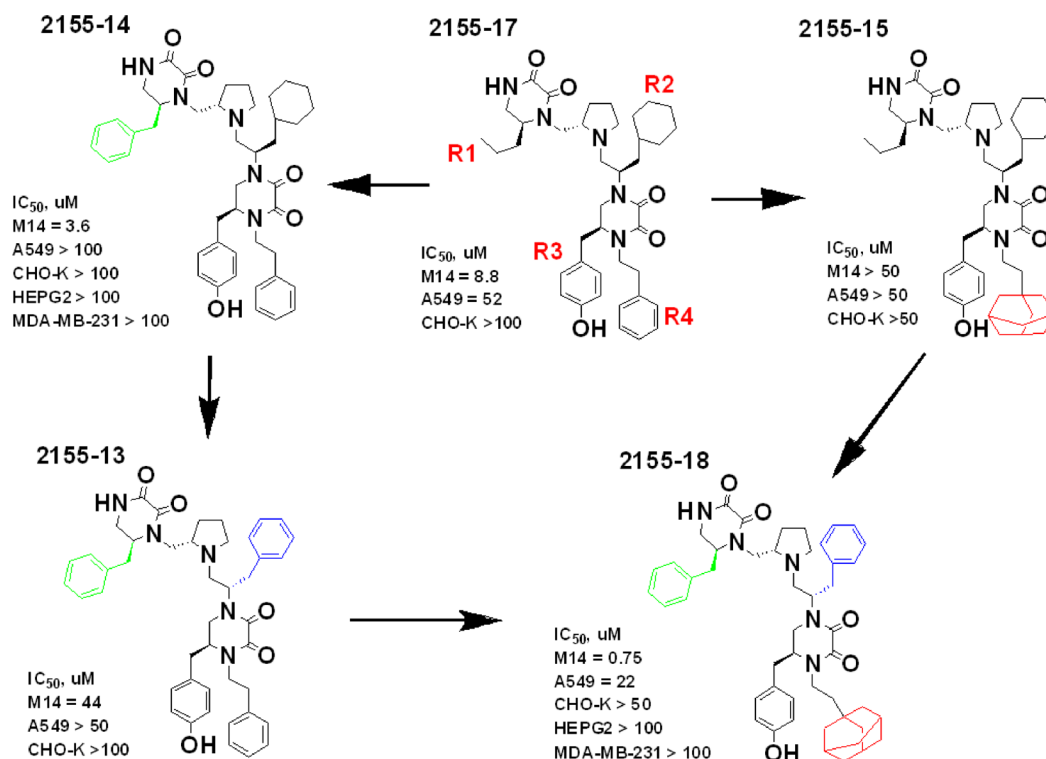


Figure 3. Optimization of pyrrolidine-bis-diketopiperazines.

moieties were examined in their place. First, we tested individual compounds with *R*-propyl in R1. Although similar to *R*-methyl in most properties, *R*-propyl is bigger, which allows probing for the effect of size in the R1 position. Also, because the positional scan did not reveal clear preferences for a particular moiety in position R4, we utilized several different functionalities: 2-phenylbutyl, phenyl-ethyl, cyclopentyl-methyl, and 2-adamantan-1-yl-methyl (Figure 2D, samples 80, 86, 106, and 118, respectively). Samples 80 and 86 were completely inactive against all three cell lines, whereas 106 and 118 inhibited all three cell lines equipotently, which allowed us to assess the importance of R4 for selectivity. None of individual compounds from this series exhibited good activity or selectivity toward M14 or A549 cells (Table 2). We also tried *R*-cyclohexyl in the R2 position in place of hydroxybenzyl. *R*-Cyclohexyl exhibited selectivity for CHO-K1 in the positional scan (Figure 2B, sample 51). Compound 2155-17 exhibited approximately 5-fold selectivity for M14 over A549 cells and more than 10-fold selectivity over CHO-K1 cells (Figure 3, IC_{50} = 8.8 ± 1.2 , 52 ± 8.3 , and $>100 \mu M$ for M14, A549, and CHO-K1 cells, respectively). Substitution for 2-adamantan-1-yl-methyl in the R4 position to produce compound 2155-15 resulted in loss of activity toward all three cell lines (IC_{50} > $50 \mu M$). Additionally, we explored *S*-benzyl in position R1, which showed some selectivity for CHO-K1 in the positional scan (Figure 2A, sample 2). 2155-14 showed improvement of selectivity for M14 cells (Figure 3, IC_{50} = $3.6 \pm 0.3 \mu M$ for M14 and $>100 \mu M$ for A549 and CHO-K1 cells). This suggested a preference for bulky aromatic functionalities in R1. However, a further increase of bulk in R1 by substituting benzyl for naphthylmethyl resulted in a loss of selectivity, as all three cell lines were inhibited close to 100% at $100 \mu M$ (data not shown). Combination of aromatic residues in R1 and R2 (*S*-benzyl) resulted in loss of activity toward M14 cells (IC_{50} = $44 \mu M$). However, introduction of 2-adamantan-1-yl-methyl into posi-

tion R4 to obtain 2155-18 resulted in improved activity toward M14 and A549 cells while maintaining selectivity for CHO-K1 cells. 2155-14 and 2155-18 also were selective against HEPG2 and MDA-MB-231 cell lines (liver and breast cancer cell lines, respectively). Interestingly, truncation of compounds of the 2155 series at each of the R1–4 positions resulted in complete loss of activity against all three cell lines (data not shown).

We were interested to see whether 2155-14 and 2155-18 could also inhibit melanoma cells carrying different mutations. Therefore, we tested 2155-14 and 2155-18 against the SKMEL-28 melanoma cell line containing V^{600E} BRAF mutation¹⁶ and B16/F10 murine metastatic melanoma containing p53 mutation.¹⁷ Both 2155-14 and 2155-18 exhibited dose-dependent inhibition of viability of all three cell lines (Table 3). 2155-14 was the most efficient against the SKMEL-28 cell

Table 3. Inhibition Profile of 2155-14 and 2155-18 with Melanoma Cell Lines Carrying Different Mutations^a

compound	M14	SKMEL-28	B16/F10
2155-14	3.6 ± 0.3	0.56 ± 0.04	2.7 ± 0.2
2155-18	0.89 ± 0.07	0.75 ± 0.06	1.15 ± 0.08

^aData are reported as the mean of three experiments \pm standard deviation. Units are IC_{50} in micromolar.

line (IC_{50} = 563 ± 40 nM, $3.6 \pm 0.3 \mu M$, and $2.7 \pm 0.2 \mu M$ for SKMEL-28, M14, and B16/F10, respectively), whereas 2155-18 inhibited all three lines equipotently (IC_{50} = 890 ± 70 , 745 ± 60 , and 1149 ± 80 nM for SKMEL-28, M14, and B16/F10 cells, respectively). Of note, 2155-14 was not able to inhibit M14 cell viability fully at the highest tested concentration ($100 \mu M$), whereas the two other cell lines were $\sim 100\%$ inhibited starting at $10 \mu M$ 2155-14. This suggests that 2155-14 may potentially act via inhibition of the MAPK pathway, which is constitutively activated in melanomas carrying V^{600E} BRAF and

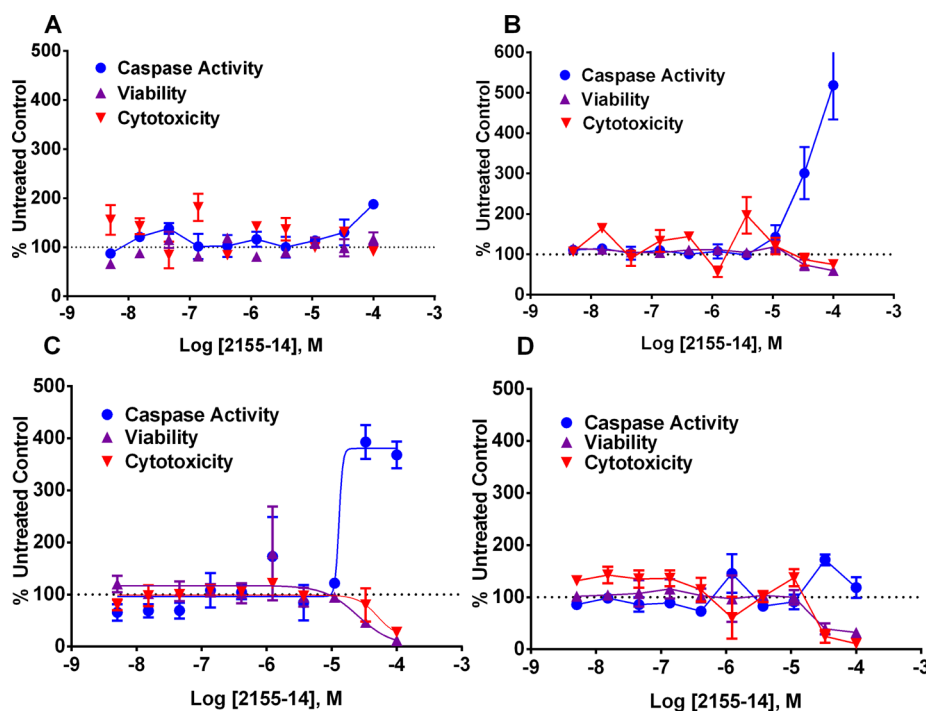


Figure 4. Results of ApoTox time-course assay: (A) 4, (B) 24, (C) 48, and (D) 72 h.

NRAS mutations.^{18,19} 2155-14 could potentially be a better inhibitor of mutant V^{600E} BRAF than the wild-type BRAF, which could explain the difference in potency toward M14 and SKMEL-28 cells. Another possibility is that 2155-14 could be acting on the HSP90 chaperone that has multiple client proteins in the MAPK pathway. Inhibition of HSP90 by small molecule (17-AAG) resulted in melanoma stabilization in patients carrying BRAF or NRAS mutation. Further studies of mechanism of action of 2155-14 and 2155-18 are required to determine their potential target(s) in melanoma.

The potency exhibited by 2155-14 and 2155-18 against the above-mentioned melanoma cell lines is comparable to vemurafenib (Zelboraf, RG7204; PLX4032; RO5185426), which is a first-in-class, specific small-molecule inhibitor of V^{600E} BRAF. Vemurafenib has been approved by the U.S. Food and Drug Administration for the treatment of late-stage (metastatic) or unresectable melanoma in patients whose tumors express V^{600E} BRAF. Vemurafenib inhibited V^{600E} BRAF-positive melanoma cell lines (i.e., M263, M321, SKMEL28, M229, M238, M249, and M262) with IC_{50} values in the 0.1–10 μ M range²⁰ but was inactive up to 10 μ M against melanoma cells with mutated Q^{61L} NRAS and wild-type BRAF (i.e., M202 and M207). The M14 (G^{12C} NRAS) cell line was inhibited by vemurafenib with a 150 nM IC_{50} .²¹

Knowledge of the mechanism of cell death caused by a lead compound can help predict potential compound liabilities and allow prioritization of compounds. For example, compounds that cause primary necrosis usually do not make good drug candidates because of their general toxicity, whereas cell-cycle inhibitors have proven to be very selective and well-tolerated in melanoma clinical trials.²² Our lead compounds were discovered as a result of a phenotypic assay; therefore, to exclude the possibility of necrosis as a mechanism of death, we performed a time-course study using the CellTiter-Glo viability assay. Primary necrosis is characterized by the rapid loss of cell viability, which can be detected as early as 3 h after compound

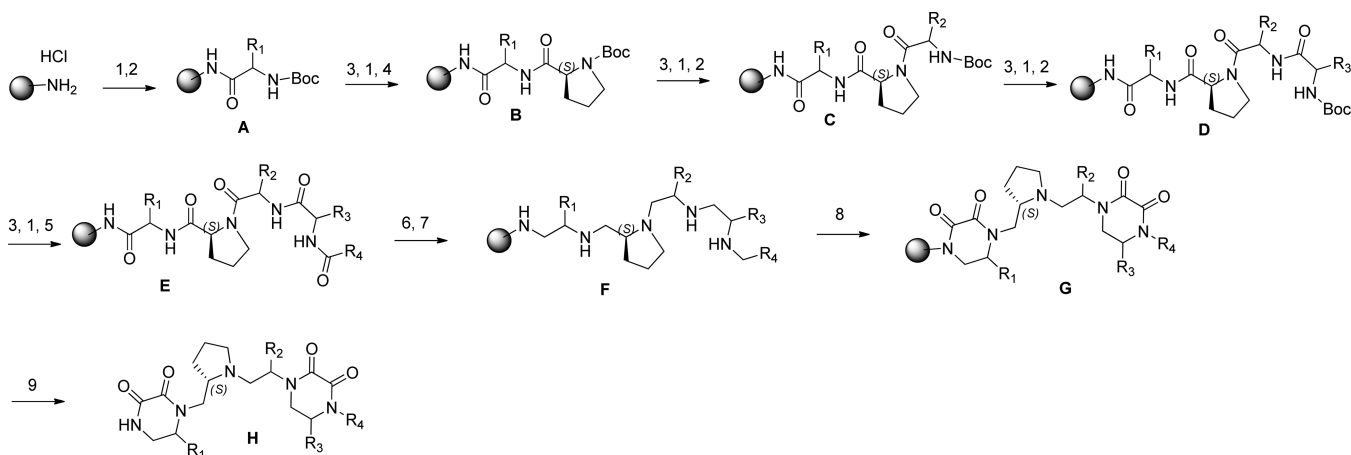
addition.²³ We determined the effect of lead compound application on the viability of M14 cells at 4, 24, 48, and 72 h. The test and control compounds (gefitinib (fast apoptosis inducer), doxorubicin (late apoptosis inducer), and ionomycin (primary necrosis inducer)) were screened in 10-point, 1:3 serial dilution dose–response format starting at 100 μ M. None of the lead compounds exhibited signs of cell viability loss at any concentration at the 4 h time point and only slight loss of viability at the 24 h time point. All compounds reached their full potency at 48 h (data not shown). These data suggested that lead compounds 2155-14 and 2155-18 are unlikely to cause primary necrosis in M14 cells.

Once we were able to exclude primary necrosis as a cell-death mechanism, we were interested in a more detailed characterization of the cellular target for our lead compounds. We utilized the ApoTox-Glo triplex assay, which allows one to assess simultaneously the effect of small molecules on cell viability, toxicity, caspase activity, and cell cycle all in the same well.²⁴

First, a mixture of two fluorogenic substrates was added to cells. The GF-AFC substrate is cell-permeant and nonlytic to cells, allowing the measurement of active protease inside live cells. The second substrate (bis-AAF-R110 substrate) is not cell-permeable and is cleaved only when proteases are released from cells as a result of the loss of membrane integrity typical of cell death. This step generates an inversely correlated measurement of cell viability and toxicity.

The second addition is luminogenic DEVD-peptide substrate for caspase-3/7 and Ultra-Glo recombinant thermostable luciferase. Caspase-3/7 cleavage of the substrate generates a luminescent signal that correlates with caspase-3/7 activation as a key indicator of apoptosis. Because markers for cytotoxicity and apoptosis are transient, the assay was conducted in time-course format with time points at 4, 24, 48, and 72 h.

Consistent with the CellTiter-Glo viability time-course experiment, compound 2155-14 exhibited no effect on cell

Scheme 2. General Synthesis Procedure of Pyrrolidine-bis-diketopiperazines^a

^a(1) 5% DIEA/95% DCM; (2) Boc-AA, DIC, HOBt, DMF; (3) 55%TFA/45%DCM; (4) Boc-L-Pro-OH, DIC, HOBt, DMF; (5) COOH, DIC, HOBt, DMF; (6) 40× BH₃/THF (65 °C, 72 h); (7) piperidine (65°C, 18hr); (8) 10× (COIm)₂ (18 h); (9) HF/Anisole, (0 °C, 1.5 h).

viability, as measured by live cell protease at the 4 h time point (Figure 4A). Additionally, there were no markers for apoptosis and cytotoxicity. This suggested a lack of effect on cell health at early time points. The 24 h time point was characterized by a significant spike in caspase activity, suggesting activation of apoptotic machinery (Figure 4B).

At 48 h, the caspase signal was decreased compared to the 24 h time point (Figure 4C, 400% of untreated control versus 550% of untreated control for 48 and 24 h, respectively). Viability and cytotoxicity showed dose-dependent responses at 48 h, suggesting loss of cell membrane integrity. By 72 h, the caspase signal has decayed, suggesting that cells had completed the apoptotic process (Figure 4D).

We compared the ApoTox profile of 2155-14 with profiles of ionomycin (primary necrosis inducer), terfenadine (fast apoptosis inducer), and panobinostat (late apoptosis inducer) (Figure S3). Ionomycin induced a strong cytotoxicity response and dose-dependent loss of viability as early as 4 h after addition to M14 cells, consistent with its mechanism of action (membrane disruption) (Figure S3A). Also, ionomycin did not induce a spike in caspase activity at any of the time points compared to the untreated control.

Terfenadine induced an early loss of cell viability and a cytotoxicity spike similar to ionomycin. However, it also exhibited an early caspase activity spike (4–24 h) characteristic of early apoptosis (Figure S3E,F).

Panobinostat had no effect on viability, cytotoxicity, or caspase activity at the 4 h time point (Figure S3I). Panobinostat has to penetrate the cell nucleus to inhibit HDACs, which results in the longer dose-to-effect time (late-onset apoptosis). Caspase activity spiked at 24–48 h accompanied by a dose-dependent loss of viability (Figure S3J,K). Cytotoxicity spiked transiently at 24 h (Figure S3J). This is consistent with what is known about panobinostat's mechanism of action, which is based on pan-HDAC inhibition.²⁵

Because 2155-14 exhibited a profile most similar to panobinostat, we hypothesized that 2155-14 and 2155-18 could potentially act via HDAC inhibition. However, testing of 2155-14 and 2155-18 with representative HDACs from class I (HDAC1 and 2) and II (HDAC6) revealed a lack of HDAC inhibition up to 100 μM (data not shown). This suggests that 2155-14 and 2155-18 either act by selectively inhibiting other

members of the HDAC family or via an entirely different mechanism. Despite the fact that 2155-14 and 2155-18 do not appear to act by HDAC inhibition, they inhibited M14 cells via inducing late-stage apoptosis, which suggests the possibility of a novel intracellular target. Lack of a cytotoxicity signal over the time course of the assay also suggested possible cell-cycle arrest.

In conclusion, we discovered and conducted initial characterization of a novel class of compounds that inhibit melanoma cell lines carrying NRAS and BRAF mutations while sparing healthy cells. The lead of the series, 2155-18, exhibited cell-based potency comparable to the FDA-approved melanoma therapy. Mechanism of death analysis suggests that these compounds act by inducing late-onset apoptosis, possibly because of the intracellular or intranuclear location of target(s). We will further characterize this novel chemotype to determine the identity of its target(s) and the possibility of utilizing this novel pyrrolidine diketopiperazine scaffold for oncological drug discovery.

It is also important to note that the screening campaign (i.e., scaffold ranking, deconvolution by positional scanning, and testing of individual compounds, all done in triplicate) required only approximately thirty 384-well plates for each cell type (CHO-K1, M14, and A549). This level of throughput requires only minimal laboratory automation while allowing assessment of 738 192 members of the pyrrolidine diketopiperazine scaffold and greater than 5 000 000 small molecules in the scaffold-ranking plate. For comparison, to screen 738 192 individual compounds in conventional HTS using the 1536-well plate format would require approximately 500–600 plates per cell line, integrated robotics, and multiple scientific and engineering staff. Overall, mixture-based phenotypic HTS can significantly reduce cost and hit-to-lead time while yielding novel compounds with promising pharmacology.

EXPERIMENTAL PROCEDURES

General Synthesis Procedure for Pyrrolidine-bis-diketopiperazine. All compounds were synthesized via solid-phase methodology (Scheme 2) on 4-methylbenzhydrylamine hydrochloride resin (MBHA) (1.1 mmol/g, 100–200 mesh) using the tea-bag approach²⁶ as previously described.²⁷ Boc-amino acids were coupled utilizing standard coupling procedures (6 equiv) with hydroxybenzotriazole hydrate (HOBt, 6 equiv) and *N,N'*-diisopropylcarbodiimide (DIC, 6 equiv) in dimethylformamide (DMF, 0.1 M) for 120 min. Boc

protecting groups were removed with 55% trifluoroacetic acid (TFA)/45% dichloromethane (DCM) (1×, 30 min) and subsequently neutralized with 5% diisopropylethylamine (DIEA)/95% DCM (3×, 2 min). Carboxylic acids (10 equiv) were coupled utilizing standard coupling procedures with HOBt (10 equiv) and DIC (10 equiv) in DMF (0.1 M) for 120 min. Completion of all couplings was monitored with a ninhydrin test. Initially, 100 mg of MBHA resin was placed inside a mesh "tea-bag", washed with DCM (2×, 1 min), neutralized with 5% DIEA/95% DCM (3×, 2 min), and then rinsed with DCM (2×, 1 min). A Boc-protected amino acid was coupled utilizing the above procedure to add R1 to the resin (Scheme 2A). Once complete, the solution was poured off, and the bags were rinsed with DMF (3×, 1 min) and DCM (3×, 1 min). The Boc protecting group was removed, and the bags were rinsed with DCM (2×, 1 min), isopropyl alcohol (IPA) (2×, 1 min), and DCM (2×, 1 min) and then neutralized. Boc-L-proline-OH was then coupled utilizing the above procedure (Scheme 2B). The process was repeated to add R2 (Scheme 2C) and R3 (Scheme 2D), and then a carboxylic acid was coupled utilizing the above procedure to add R4 (Scheme 2E). Compounds were reduced to F (Scheme 2F) using a 40× excess of borane (1.0 M in tetrahydrofuran (THF)) over each amide bond in a glass vessel under nitrogen at 65 °C for 72 h. The solution was then poured off, the reaction was quenched with methanol (MeOH), and the bags were washed with THF (1×, 1 min) and MeOH (4×, 1 min) and allowed to air-dry. Once dry, the bags were treated with piperidine overnight at 65 °C in a glass vessel. The solution was poured off, and the bags were washed with DMF (2×, 1 min), DCM (2×, 1 min), MeOH (1×, 1 min), DMF (2×, 1 min), DCM (2×, 1 min), and MeOH (1×, 1 min) and allowed to air-dry. Completion of reduction was checked by cleaving a control sample and analyzing using LCMS. Diketopiperazine cyclization (Scheme 2G) was performed under anhydrous conditions (<22% humidity). The dry bags were washed with anhydrous DMF (2×, 1 min), added to a solution of 1,1'-oxalylidiimidazole (5-fold excess for each cyclization site) in anhydrous DMF (0.1 M), and shaken at room temperature overnight. The solution was poured off, and the bags were rinsed with DMF (3×, 1 min) and DCM (3×, 1 min). Completion of cyclization was checked by cleaving a control sample and analyzing by LCMS. The compounds were then cleaved from the resin with hydrofluoric acid (HF) in the presence of anisole in an ice bath at 0 °C for 90 min (Scheme 2H) and extracted using 95% acetic acid (AcOH)/5% H₂O (2×, 5 mL). Final crude products were purified using HPLC as described above. All chirality was generated from the corresponding amino acids. Under the reaction conditions described, no epimerization was observed, and for those compounds with multiple chiral centers, a single diastereomer was obtained.

Compound Purification and Characterization. All reagents were commercially available and used without further purification. The final compounds were purified using preparative HPLC with a dual-pump Shimadzu LC-20AB system equipped with a Luna C18 preparative column (21.5 × 150 mm, 5 μm) at λ = 214 nm, with a mobile phase of (A) H₂O (+0.1% formic acid)/(B) acetonitrile (ACN) (+0.1% formic acid) at a flow rate of 13 mL/min; gradients varied by compound and were based on hydrophobicity. ¹H NMR and ¹³C NMR spectra were recorded in DMSO-*d*₆ on a Bruker Ascend 400 MHz spectrometer at 400.14 and 100.62 MHz, respectively, and MALDI-TOF mass spectra were recorded using an Applied Biosystems Voyager DE-PRO biospectrometry workstation. The purities of synthesized compounds were confirmed to be greater than 95% by liquid chromatography and mass spectrometry on a Shimadzu LCMS-2010 instrument with ESI mass spec and SPD-20A liquid chromatograph with a mobile phase of (A) H₂O (+0.1% formic acid)/(B) ACN (+0.1% formic acid) (S–95% over 6 min with a 4 min rinse).

Synthesis of Positional Scanning Library 1344. Positional scanning library 1344 was synthesized as described in Scheme 2. Positional scanning library 1344 utilized both individual and mixtures of amino acids (R1, R2, and R3) and carboxylic acids (R4). The synthetic technique and subsequent screening facilitates the generation of information regarding the likely activity of individual compounds

contained in the library.^{1,9,10} The equimolar isokinetic ratios utilized for the mixtures were previously determined and calculated for each of the amino acids and carboxylic acids.^{28,29} Library 1344 has a total diversity of 738 192 compounds (26 × 26 × 26 × 42 = 738 192). The R1, R2, and R3 positions, as shown in Scheme 2H, each consisted of 26 amino acids, and the R4 position contained 42 carboxylic acids. By way of example, sample 2 (Figure 2) contains an equal molar amount of all 28 392 individual compounds in library 1344 that have *S*-benzyl fixed at the R1 position, and likewise sample 28 contains an equal molar amount of all 28 392 individual compounds in library 1344 that have *S*-benzyl fixed at the R2 position.

Scaffold-Ranking Library. The scaffold-ranking library contained one sample for each of the 37 positional scanning libraries tested. Each of these samples contained an approximate equal molar amount of each compound in that library. So, for example, scaffold-ranking library 1344 contained 738 192 pyrrolidine-bis-diketopiperazines in approximately equal molar amounts. Each of these 37 mixture samples can be prepared by mixing the cleaved products of the complete positional scanning library, as was the case for 1344, or they can be synthesized directly as a single mixture.^{1,30}

TPIMS Mixture Library Screening. Mixture libraries were solubilized in 3% DMSO/H₂O and added to polypropylene 384-well plates (Greiner cat. no. 781280). CHO-K1, A549, or M14 cells (1250) were plated in 384-well plates in 5 μL of serum-free media (F12 for CHO-K1 and A549, DMEM for M14). Test compounds and gefitinib (pharmacological assay control) were prepared as 10-point, 1:3 serial dilutions starting at 300 μM and were then added to the cells (5 μL per well) using the Biomek NX³. Plates were incubated for 72 h at 37 °C, 5% CO₂, and 95% RH. After incubation, 5 μL of CellTiter-Glo (Promega cat. no. G7570) was added to each well, and plates were incubated for 15 min at room temperature. Luminescence was recorded using a Biotek Synergy H4 multimode microplate reader. Viability was expressed as a percentage relative to wells containing media only (0%) and wells containing cells treated with 1% DMSO only (100%). Three parameters were calculated on a per-plate basis: (a) the signal-to-background ratio (S/B), (b) the coefficient for variation (CV; CV = (standard deviation/mean)100) for all compound test wells, and (c) the Z' factor (18). The IC₅₀ value of the pharmacological control (gefitinib, LC Laboratories no. G-4408) was also calculated to ascertain the assay's robustness.

The time-course viability assay was performed as described for library screening, with luminescence measurements performed at 4, 24, 48, and 72 h.

Hexosaminidase Viability Assay. Hexosaminidase assay was used to study the effects of 2155-14 and 2155-18 on cell viability or cell proliferation of both B16/F-10 and SKMEL-28 cells.³¹ In brief, cells were plated in 96-well plates, grown overnight, and treated the next day with increasing concentrations of compounds (0–50 μM) for 48 h. After 48 h of treatment, media was discarded, and cells were washed with PBS to remove residual media from wells. Hexosaminidase substrate (75 μL) (Sigma-Aldrich; cat. no. N9376) was added to each well and incubated at 37 °C for 30 min followed by addition of 112.5 μL of developer into each well. Final absorbance was measured at λ = 405 nm. Cell growth was calculated as percent viability = (A/B)100, where A and B are the absorbance of treated and control cells, respectively.

Luciferase Counterscreen Assay. Lead compounds were tested for inhibition of luciferase from the CellTiter-Glo assay kit (Promega cat. no. G7570). The ATP concentration in the luciferase assay was matched to the response produced by M14 cells. Test compounds were prepared as 10-point, 1:3 serial dilutions starting at 300 μM and were then added to the DMEM (5 μL per well) using the Biomek NX³. Plates were incubated for 1 h at 37 °C, 5% CO₂, and 95% RH. After incubation, 5 μL of CellTiter-Glo was added to each well, and incubation continued for 15 min at room temperature. Luminescence was recorded using a Biotek Synergy H4 multimode microplate reader. Inhibition was expressed as a percentage relative to wells containing media only (0%) and wells containing CellTiter-Glo (100%).

ApoTox-Glo Triplex Assay. M14 #5 cells were plated in 384-well format at a density of 1250 cells in 5 μL of serum-free DMEM media

and incubated at 37 °C in 5% CO₂ for 4 h. Control and test compounds were serially diluted in a ratio of 1:3 and added to wells in 4 μ L. Ionomycin, terfenadine, and panobinostat were used as controls for the mechanism of cell death. Plates were incubated at 37 °C in 5% CO₂ for 4, 24, 48, and 72 h. At the end of each time point, viability/cytotoxicity reagent was prepared containing 400 μ M glycyphenylalanyl-aminofluorocoumarin (GF-AFC) substrate (cleavable by live cell proteases) and 400 μ M bis-alanylalanyl-phenylalanyl-rhodamine 110 (bis-AAF-R110) substrate (cleavable by dead cell proteases). Four microliters of the viability/cytotoxicity reagent was used per well. The plate was incubated for 30 min at 37 °C. Fluorescence was read at λ_{Ex} = 400 nm and λ_{Em} = 505 nm for GF-AFC and λ_{Ex} = 485 nm and λ_{Em} = 520 nm for bis-AAF-R110 on the BioTek Synergy 4 multi-mode microplate reader. Caspase-Glo 3/7 reagent was then added in a 12 μ L volume. The plate was incubated for 30 min at room temperature, and luminescence was measured on the BioTek Synergy 4 multi-mode microplate reader.

■ ASSOCIATED CONTENT

■ Supporting Information

¹H and ¹³C NMR, LCMS, and results of ApoTox assay with assay controls. This material is available free of charge via the Internet at <http://pubs.acs.org>.

■ AUTHOR INFORMATION

Corresponding Author

*E-mail: dminond@tpims.org; Phone: 772-345-4705; Fax: 772-345-3649.

Author Contributions

The manuscript was written by D.M. with contributions by M.G. and T.L. and was edited by G.B.F. All authors have given approval to the final version of the manuscript.

Notes

The authors declare no competing financial interest.

■ ACKNOWLEDGMENTS

This work was supported by the James and Esther King Biomedical Research Program (2KN05 to D.M.), the National Institutes of Health (DA033985 to D.M., CA098799 to G.B.F., and DA031370 to R.A.H.), the Multiple Sclerosis National Research Institute (to G.B.F.), and the State of Florida, Executive Office of the Governor's Office of Tourism, Trade, and Economic Development. We acknowledge Drs. Kara Chamberlain and Andrew Niles for ApoTox technology-related discussions.

■ ABBREVIATIONS USED

HTS, high-throughput screening

■ REFERENCES

- (1) Houghten, R. A.; Pinilla, C.; Giulianotti, M. A.; Appel, J. R.; Dooley, C. T.; Nefzi, A.; Ostresh, J. M.; Yu, Y.; Maggiora, G. M.; Medina-Franco, J. L.; Brunner, D.; Schneider, J. Strategies for the use of mixture-based synthetic combinatorial libraries: Scaffold ranking, direct testing in vivo, and enhanced deconvolution by computational methods. *J. Comb. Chem.* **2008**, *10*, 3–19.
- (2) Lee, J. A.; Berg, E. L. Neoclassic drug discovery: The case for lead generation using phenotypic and functional approaches. *J. Biomol. Screening* **2013**, *18*, 1143–1155.
- (3) Swinney, D. C.; Anthony, J. How were new medicines discovered? *Nat. Rev. Drug Discovery* **2011**, *10*, 507–519.
- (4) Tentori, L.; Lacal, P. M.; Graziani, G. Challenging resistance mechanisms to therapies for metastatic melanoma. *Trends Pharmacol. Sci.* **2013**, *34*, 656–666.
- (5) Medina-Franco, J. L.; Giulianotti, M. A.; Welmaker, G. S.; Houghten, R. A. Shifting from the single to the multitarget paradigm in drug discovery. *Drug Discovery Today* **2013**, *18*, 495–501.
- (6) Paolini, G. V.; Shapland, R. H.; van Hoorn, W. P.; Mason, J. S.; Hopkins, A. L. Global mapping of pharmacological space. *Nat. Biotechnol.* **2006**, *24*, 805–815.
- (7) Reifemberger, J.; Knobbe, C. B.; Sterzinger, A. A.; Blaschke, B.; Schulte, K. W.; Ruzicka, T.; Reifemberger, G. Frequent alterations of Ras signaling pathway genes in sporadic malignant melanomas. *Int. J. Cancer* **2004**, *109*, 377–384.
- (8) Bennett, D. C.; Charest, J.; Sebolt, K.; Lehrman, M.; Rehemtulla, A.; Contessa, J. N. High-throughput screening identifies aclacinomycin as a radiosensitizer of EGFR-mutant non-small cell lung cancer. *Transl. Oncol.* **2013**, *6*, 382–391.
- (9) Rideout, M. C.; Boldt, J. L.; Vahi-Ferguson, G.; Salamon, P.; Nefzi, A.; Ostresh, J. M.; Giulianotti, M.; Pinilla, C.; Segall, A. M. Potent antimicrobial small molecules screened as inhibitors of tyrosine recombinases and Holliday junction-resolving enzymes. *Mol. Diversity* **2011**, *15*, 989–1005.
- (10) Reilley, K. J.; Giulianotti, M.; Dooley, C. T.; Nefzi, A.; McLaughlin, J. P.; Houghten, R. A. Identification of two novel, potent, low-liability antinociceptive compounds from the direct in vivo screening of a large mixture-based combinatorial library. *AAPS J.* **2010**, *12*, 318–329.
- (11) Wu, J.; Zhang, Y.; Maida, L. E.; Santos, R. G.; Welmaker, G. S.; Lavoie, T. M.; Nefzi, A.; Yu, Y.; Houghten, R. A.; Toll, L.; Giulianotti, M. A. Scaffold ranking and positional scanning utilized in the discovery of nAChR-selective compounds suitable for optimization studies. *J. Med. Chem.* **2013**, *56*, 10103–10117.
- (12) Ranjit, D. K.; Rideout, M. C.; Nefzi, A.; Ostresh, J. M.; Pinilla, C.; Segall, A. M. Small molecule functional analogs of peptides that inhibit lambda site-specific recombination and bind Holliday junctions. *Bioorg. Med. Chem. Lett.* **2010**, *20*, 4531–4544.
- (13) Minond, D.; Cudic, M.; Bionda, N.; Giulianotti, M.; Maida, L.; Houghten, R. A.; Fields, G. B. Discovery of novel inhibitors of a disintegrin and metalloprotease 17 (ADAM17) using glycosylated and non-glycosylated substrates. *J. Biol. Chem.* **2012**, *287*, 36473–36487.
- (14) Houghten, R. A.; Pinilla, C.; Appel, J. R.; Blondelle, S. E.; Dooley, C. T.; Eichler, J.; Nefzi, A.; Ostresh, J. M. Mixture-based synthetic combinatorial libraries. *J. Med. Chem.* **1999**, *42*, 3743–3778.
- (15) Pinilla, C.; Appel, J. R.; Blanc, P.; Houghten, R. A. Rapid identification of high affinity peptide ligands using positional scanning synthetic peptide combinatorial libraries. *Biotechniques* **1992**, *13*, 901–915.
- (16) Xing, F.; Persaud, Y.; Pratilas, C. A.; Taylor, B. S.; Janakiraman, M.; She, Q. B.; Gallardo, H.; Liu, C.; Merghoub, T.; Hefter, B.; Dolgalev, I.; Viale, A.; Heguy, A.; De Stanchina, E.; Cobrinik, D.; Bollag, G.; Wolchok, J.; Houghten, A.; Solit, D. B. Concurrent loss of the PTEN and RB1 tumor suppressors attenuates RAF dependence in melanomas harboring (V600E)BRAF. *Oncogene* **2012**, *31*, 446–457.
- (17) Castle, J. C.; Kreiter, S.; Diekmann, J.; Lower, M.; van de Roemer, N.; de Graaf, J.; Selmi, A.; Diken, M.; Boegel, S.; Paret, C.; Koslowski, M.; Kuhn, A. N.; Britten, C. M.; Huber, C.; Tureci, O.; Sahin, U. Exploiting the mutanome for tumor vaccination. *Cancer Res.* **2012**, *72*, 1081–1091.
- (18) Jang, S.; Atkins, M. B. Which drug, and when, for patients with BRAF-mutant melanoma? *Lancet Oncol.* **2013**, *14*, e60–69.
- (19) Banerji, U.; Affolter, A.; Judson, I.; Marais, R.; Workman, P. BRAF and NRAS mutations in melanoma: Potential relationships to clinical response to HSP90 inhibitors. *Mol. Cancer Ther.* **2008**, *7*, 737–749.
- (20) Sondergaard, J. N.; Nazarian, R.; Wang, Q.; Guo, D.; Hsueh, T.; Mok, S.; Sazegar, H.; MacConaill, L. E.; Barretina, J. G.; Kehoe, S. M.; Attar, N.; von Eeuw, E.; Zuckerman, J. E.; Chmielowski, B.; Comin-Anduix, B.; Koya, R. C.; Mischel, P. S.; Lo, R. S.; Ribas, A. Differential sensitivity of melanoma cell lines with BRAFV600E mutation to the specific Raf inhibitor PLX4032. *J. Transl. Med.* **2010**, *8*, 29–39.
- (21) Yadav, V.; Zhang, X.; Liu, J.; Estrem, S.; Li, S.; Gong, X. Q.; Buchanan, S.; Henry, J. R.; Starling, J. J.; Peng, S. B. Reactivation of

mitogen-activated protein kinase (MAPK) pathway by FGF receptor 3 (FGFR3)/Ras mediates resistance to vemurafenib in human B-RAF V600E mutant melanoma. *J. Biol. Chem.* **2012**, *287*, 28087–28098.

(22) Sheppard, K. E.; McArthur, G. A. The cell-cycle regulator CDK4: An emerging therapeutic target in melanoma. *Clin. Cancer Res.* **2013**, *19*, 5320–5328.

(23) Nicotera, P.; Leist, M.; Manzo, L. Neuronal cell death: A demise with different shapes. *Trends Pharmacol. Sci.* **1999**, *20*, 46–51.

(24) Niles, A. L.; Moravec, R. A.; Riss, T. L. In vitro viability and cytotoxicity testing and same-well multi-parametric combinations for high throughput screening. *Curr. Chem. Genomics* **2009**, *3*, 33–41.

(25) Atadja, P. Development of the pan-DAC inhibitor panobinostat (LBH589): Successes and challenges. *Cancer Lett.* **2009**, *280*, 233–241.

(26) Houghten, R. A. General method for the rapid solid-phase synthesis of large numbers of peptides: Specificity of antigen-antibody interaction at the level of individual amino acids. *Proc. Natl. Acad. Sci. U.S.A.* **1985**, *82*, 5131–5135.

(27) Pinilla, C.; Edwards, B. S.; Appel, J. R.; Yates-Gibbins, T.; Giulianotti, M. A.; Medina-Franco, J. L.; Young, S. M.; Santos, R. G.; Sklar, L. A.; Houghten, R. A. Selective agonists and antagonists of formylpeptide receptors: Duplex flow cytometry and mixture-based positional scanning libraries. *Mol. Pharmacol.* **2013**, *84*, 314–324.

(28) Acharya, A. N.; Ostresh, J. M.; Houghten, R. A. Determination of isokinetic ratios necessary for equimolar incorporation of carboxylic acids in the solid-phase synthesis of mixture-based combinatorial libraries. *Biopolymers* **2002**, *65*, 32–39.

(29) Ostresh, J. M.; Winkle, J. H.; Hamashin, V. T.; Houghten, R. A. Peptide libraries: Determination of relative reaction rates of protected amino acids in competitive couplings. *Biopolymers* **1994**, *34*, 1681–1689.

(30) Santos, R. G.; Appel, J. R.; Giulianotti, M. A.; Edwards, B. S.; Sklar, L. A.; Houghten, R. A.; Pinilla, C. The mathematics of a successful deconvolution: A quantitative assessment of mixture-based combinatorial libraries screened against two formylpeptide receptors. *Molecules* **2013**, *18*, 6408–6424.

(31) Landegren, U. Measurement of cell numbers by means of the endogenous enzyme hexosaminidase. Applications to detection of lymphokines and cell surface antigens. *J. Immunol. Methods* **1984**, *67*, 379–388.

■ NOTE ADDED AFTER ASAP PUBLICATION

This paper was published ASAP on February 5, 2014. The spelling of Lillian Onwuha-Ekpete's name has been corrected and the revised version was reposted on February 10, 2014.